HHS Public Access

Author manuscript

Anal Chem. Author manuscript; available in PMC 2024 February 02.

Published in final edited form as:

Anal Chem. 2023 December 12; 95(49): 18039–18045. doi:10.1021/acs.analchem.3c02405.

Top/Middle-Down Characterization of α-Synuclein Glycoforms

Samuel A. Miller[∇],
Department of Chemistry and Biochemistry and Biomolecular Sciences Institute, Florida International University, Miami, Florida 33199, United States

Kevin Jeanne Dit Fouque[∇],
Department of Chemistry and Biochemistry and Biomolecular Sciences Institute, Florida International University, Miami, Florida 33199, United States

Eldon R. Hard,
Department of Chemistry and Biological Sciences, University of Southern California, Los Angeles, California 90007, United States

Aaron T. Balana,
Department of Chemistry and Biological Sciences, University of Southern California, Los Angeles, California 90007, United States

Desmond Kaplan,
KapScience LLC, Tewksbury, Massachusetts 01876, United States

Valery G. Voinov,
e-MSion Inc., Corvallis, Oregon 97330, United States

Mark E. Ridgeway,
Bruker Daltonics Inc., Billerica, Massachusetts 01821, United States

Melvin A. Park,
Bruker Daltonics Inc., Billerica, Massachusetts 01821, United States

Gordon A. Anderson,
GAA Custom Electronics, Kennewick, Washington 99338, United States

Matthew R. Pratt,
Department of Chemistry and Biological Sciences, University of Southern California, Los Angeles, California 90007, United States

Corresponding Author: Francisco Fernandez-Lima − Department of Chemistry and Biochemistry and Biomolecular Sciences Institute, Florida International University, Miami, Florida 33199, United States; fernandf@fiu.edu.

[∇]S.A.M. and K.J.D.F. contributed equally to this work.

Author Contributions

The manuscript was written through contributions of all authors. All authors have given approval to the final version of the manuscript.

Complete contact information is available at: https://pubs.acs.org/10.1021/acs.analchem.3c02405

Supporting Information

The Supporting Information is available free of charge at https://pubs.acs.org/doi/10.1021/acs.analchem.3c02405.

Additional Figures that illustrate the schematic of the nESI-UVPD-TIMS-q-ECD-ToF MS/MS instrument, Top-down ECD spectra of the $[M + 11H]^{11+}$ species, and UVPD spectra without mass isolation of intact α-synuclein unmodified, GlcNAcT72, GlcNAcT75, GlcNAcT81, and GlcNAcS87 glycoforms, and TIMS-ECD analysis of the selected $[M + 4H]^{4+}$ species of GlcNAcT72 and GlcNAcT81 (PDF)

The authors declare no competing financial interest.

Francisco Fernandez-Lima
Department of Chemistry and Biochemistry and Biomolecular Sciences Institute, Florida International University, Miami, Florida 33199, United States

Abstract

α-Synuclein is an intrinsically disordered protein that plays a critical role in the pathogenesis of neurodegenerative disorders, such as Parkinson's disease. Proteomics studies of human brain samples have associated the modification of the O-linked *N*-acetyl-glucosamine (O-GlcNAc) to several synucleinopathies; in particular, the position of the O-GlcNAc can regulate protein aggregation and subsequent cell toxicity. There is a need for site specific O-GlcNAc α-synuclein screening tools to direct better therapeutic strategies. In the present work, for the first time, the potential of fast, high-resolution trapped ion mobility spectrometry (TIMS) preseparation in tandem with mass spectrometry assisted by an electromagnetostatic (EMS) cell, capable of electron capture dissociation (ECD), and ultraviolet photodissociation (213 nm UVPD) is illustrated for the characterization of α-synuclein positional glycoforms: T72, T75, T81, and S87 modified with a single O-GlcNAc. Top-down 213 nm UVPD and ECD MS/MS experiments of the intact proteoforms showed specific product ions for each α-synuclein glycoforms associated with the O-GlcNAc position with a sequence coverage of ~68 and ~82%, respectively. TIMS-MS profiles of α-synuclein and the four glycoforms exhibited large structural heterogeneity and signature patterns across the 8+−15+ charge state distribution; however, while the α-synuclein positional glycoforms showed signature mobility profiles, they were only partially separated in the mobility domain. Moreover, a middle-down approach based on the Val40-Phe94 (55 residues) chymotrypsin proteolytic product using tandem TIMS-q-ECD-TOF MS/MS permitted the separation of the parent positional isomeric glycoforms. The ECD fragmentation of the ion mobility and m/z separated isomeric Val40-Phe94 proteolytic peptides with single O-GlcNAc in the T72, T75, T81, and S87 positions provided the O-GlcNAc confirmation and positional assignment with a sequence coverage of ~80%. This method enables the high-throughput screening of positional glycoforms and further enhances the structural mass spectrometry toolbox with fast, high-resolution mobility separations and 213 nm UVPD and ECD fragmentation capabilities.

Graphical Abstract

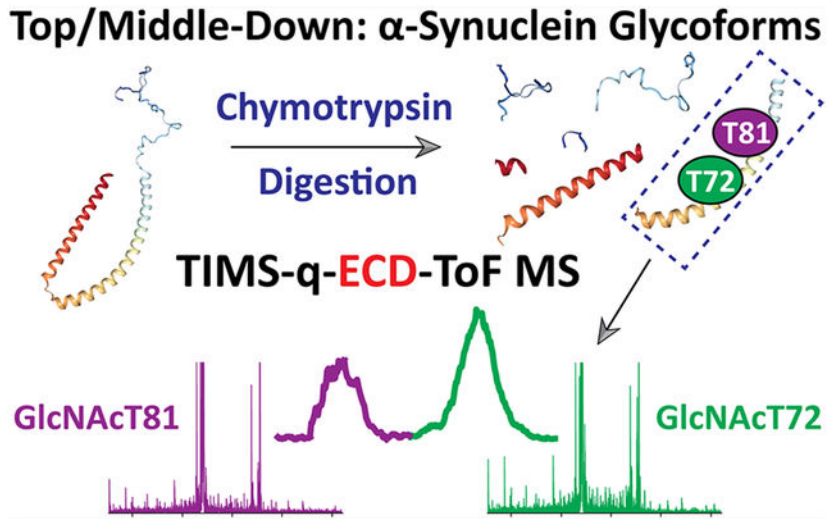

INTRODUCTION

α-Synuclein is an intrinsically disordered protein of 14.5 kDa (140 residues, Figure 1a) that is highly expressed in neurons and plays a critical role in regulating neurotransmitter release for normal brain function.[1,2] This 140 amino acid residue protein can be divided in three distinct domains, including a N-terminal amphipathic (1−60 residues, highlighted in blue in Figure 1a), a disordered acidic C-terminal (95−140 residues, highlighted in red), and a hydrophobic nonamyloid β-component (NAC, 61−94 residues, highlighted in yellow) regions.[1,3] The N-terminal amphipathic domain is a positively charged region (lysine-rich) defined by a helical folding propensity, which plays a major role for membrane binding.[4,5] The C-terminal acidic domain is a highly negatively charged region that modulates α-synuclein aggregation and binds protein partners, small molecules, and metal ions.[6,7] The NAC central domain of α-synuclein contains a highly hydrophobic motif, which is responsible for promoting fibril formation and protein aggregation.[8] α-Synucleins are mostly monomeric in healthy cells but can misfold and aggregate into oligomers and fibrils, which are toxic to cells and can disrupt normal cellular function.[1,3,9] The accumulation of α-synuclein toxic aggregates in brain cells has been associated with neurodegenerative disorders, such as Parkinson's disease,[10–12] Alzheimer's disease,[13,14] and dementia with Lewy bodies (DLB).[15,16] Understanding the mechanisms of α-synuclein aggregation and developing new therapeutic targets are still active areas of research in neuroscience. A compelling link has emerged between the α-synuclein post-translational modification (PTM) via O-linked *N*-acetyl-glucosamine (O-GlcNAc, Figure 1b) and its aggregation, for which O-GlcNAc plays an important role in the regulation of α-synuclein toxicity by preventing protein aggregation.[17–19] In fact, diverse *ex vivo* and *in vivo* studies from mouse and human models have contributed to identify up to nine different sites of O-GlcNAc modification on α-synuclein, for which several are located within the protein aggregation NAC region (highlighted in yellow in Figure 1a).[20–24] In addition, a recent study demonstrated that ~20% of total synuclein is O-GlcNAc modified in a mouse model that expresses human synuclein.[25] Therefore, the comprehensive characterization of O-GlcNAc α-synuclein glycoforms of the O-GlcNAc is of high interest to gain a better

understanding of the mechanisms for preventing protein aggregation that can be used as a potential therapeutic strategy in neurodegenerative diseases.

The biological complexity and dynamic nature of α-synuclein make their study challenging using traditional biochemical techniques. Mass spectrometry (MS) using proteomic approaches has emerged as a powerful tool for the structural characterization of α-synuclein, allowing for the identification and quantification of the post-translational modifications,[19,26,27] interactions with other proteins,[28,29] and structural changes upon protein aggregation.[30,31] In particular, the development and advancement of electron-based fragmentation (ExD)[32–34] techniques have greatly improved the middle- and top-down approaches by increasing the sequence coverage as well as the level of confidence in assigning binding partners and the nature/position of labile PTMs, such as O-GlcNAc.[19,35–38] The successful implementation of the electromagnetostatic (EMS)[39,40] cell in widespread MS platforms (e.g., quadrupole,[41–43] q-ToF,[44,45] and Orbitrap[46,47] mass spectrometers) has made electron capture dissociation (ECD) more accessible and cost-effective for proteomic analysis.

Top-down MS workflows have increasingly adopted ion mobility spectrometry in tandem with mass spectrometry (IMS-MS/MS) due to its superior speed and selectivity as compared to traditional liquid chromatography-based approaches.[48–51] The EMS cell has recently been incorporated into commercially available IMS-MS-based platforms (e.g., Agilent DTIMS-q-ToF MS,[52] Waters q-TWIMS-ToF MS,[53] and Bruker TIMS-q-ToF MS[54]) and showed the benefit of combining IMS with ECD for a comprehensive protein structural characterization. Notably, the recent integration of the EMS cell into a TIMS-q-ToF MS instrument has shown significant potential in separating and distinguishing isomeric and isobaric histone proteoforms at the middle-down level.[54,55]

In the present work, for the first time, the potential of fast, high-resolution trapped ion mobility spectrometry (TIMS) in tandem with mass spectrometry assisted by an EMS cell, capable of ECD, and UVPD is illustrated for the characterization of α-synuclein positional glycoforms. Mobility-dependent ECD and UVPD MS/MS separation is showcased for the first time for positional isomers of α-synuclein with single O-GlcNAc modifications (e.g., T72, T75, T81, and S87, Figure 1). In the following discussion, a special emphasis is placed on the comparison between the top-down and middle-down results based on the potential for ion mobility separation, PTM assignments, and sequence coverage for α-synuclein positional isomer glycoforms.

EXPERIMENTAL SECTION

Materials and Reagents.

Four positional α-synuclein isomers with a single O-GlcNAc modification in biologically relevant positions (e.g., T72, T75, T81, and S87) and the unmodified protein (Figure 1) were synthesized using the expressed protein ligation methodology, as previously described.[56] The α-synuclein glycoforms were analyzed at a concentration of 15 μM in 100 mM aqueous ammonium acetate (NH_4Ac), obtained from Fisher Scientific (Pittsburgh, PA). Middle-down glycoforms were generated by digestion with chymotrypsin, resulting in the formation of

seven peptides that are 7−86 residues in length. Low-concentration Tuning Mix standard (G1969–85000), obtained from Agilent Technologies (Santa Clara, CA), was used for external ion mobility and mass calibration of the TIMS-ToF MS instrument.

UVPD-TIMS-q-ECD-ToF MS Instrumentation.

The TIMS, ECD, and UVPD capabilities were integrated into a Bruker Maxis Impact II ToF MS (Bruker Daltonics Inc., Billerica, MA) instrument equipped with a nESI source, as depicted in Figure S1. A detailed layout of this experimental apparatus is described elsewhere.[55,57] nESI emitters were pulled in-house from quartz capillaries (O.D. = 1.0 mm and I.d. = 0.70 mm) using a Sutter Instruments Co. P2000 laser puller (Sutter Instruments, Novato, CA). Protein solutions were loaded in a pulled-tip capillary housed in a mounted custom-built XYZ stage in front of the MS inlet; the nESI emitters contained a tungsten wire biased at ~1000 V relative to the MS inlet.

A custom-built 19 mm long EMS (e-MSion Inc., Corvallis, OR) cell was attached to a custom-built collision cell and mounted between the quadrupole exit and pulsing plates of the ToF MS instrument (Figure S1). The filament was operated at a current of 2.5 A. The collision cell was operated by using high-purity argon (oxygen free) to enhance the cooling of the ions. Additional details on the ECD operation are described elsewhere.[54,58] ECD spectra were collected on quadrupole isolated (mass window of 5 Da) precursor ions, where each of the ECD events was synchronized with the ion mobility scan step, allowing for precursor-fragment ion mobility alignment. UVPD experiments were performed using a 213 nm laser beam generated from the fifth harmonic of a Nd:YAG laser (NL204, EKSPLA, Vilnius, Lithuania). The UV laser was aligned with a 203 mm long UVPD linear ion trap (quadrupolar design) incorporated prior to the TIMS 2 analyzer and operated at a repetition rate of 1 kHz with an energy of ~0.2 mJ per pulse (Figure S1). Additional details on the UVPD operation can be found elsewhere.[55,57] UVPD spectra were collected without mass isolation; molecular ions were UV irradiated with ~155 laser pulses in the UVPD trap. 2D-UVPD-TIMS-MS/MS and 2D-TIMS-q-ECD MS/MS spectra were summed every 15.5 s (100 acquisitions of 155 ms) and averaged for 50 (~13 min) and 100 (~25 min) frames, respectively. The UVPD/ECD spectra were deconvoluted using *UniDec*[59] *v4.4.0*, and assignments were performed using *ProSight Lite v1.4*. The UVPD/ECD spectra were annotated with a mass error of <20 ppm with a $S/N > 4$.

The general fundamentals of TIMS as well as the calibration procedure have been described in the literature.[60–63] TIMS experiments were carried out using nitrogen (N_2) as buffer gas, at ambient temperature (T) with a gas velocity defined by the funnel entrances (P_1 = 3.9 mbar/P_3 = 2.1 mbar) and exits (P_2 = 2.6 mbar/P_4 = 0.74 mbar) pressure differences (Figure S1). TIMS 1 was operated in transmission mode (rf voltage of 160 Vpp at 755 kHz). Ion mobility separation of the intact α-synuclein glycoforms and middle-down peptides was performed in TIMS2 (rf voltage of 250Vpp at 880 kHz). A deflector voltage of 300 V, a TIMS 1 voltage of 170 V, a TIMS exit lens (gate 1) of 169 V, a multipole exit lens (gate 2) of 135 V, and a TIMS 2 ramp voltage of −150 to −50 V were used for all the experiments (Figure S1). The scan rate ($Sr = \Delta V_{ramp}/t_{ramp}$) was optimized for the binary mixtures to maximize the ion mobility separation.

RESULTS AND DISCUSSION

TIMS-MS Analysis of α-Synuclein Glycoforms.

The nESI-MS analysis of the unmodified α-synuclein (~14.5 kDa) and the four GlcNAc α-synuclein glycoforms (~14.7 kDa) in native-like solution conditions (i.e., 100 mM aqueous NH_4Ac), exhibited a broad charge state distribution ranging from $[M + 8H]^{8+}$ to $[M + 15H]^{15+}$ molecular ions species, centered at 11+ (Figure 2a). The presence of a wide charge state distribution was streamlined as a structural change in the native-like protein states (folded conformations) toward more elongated structures, probably due to exposure of the basic residues (lysine-rich protein) together with the presence of an unrestricted C-terminal domain (highlighted in red in Figure 1a).

In addition, the TIMS mobility profiles of the unmodified α-synuclein and the four GlcNAc α-synuclein glycoforms (Figure 2b) exhibited large structural heterogeneity over a wide collision cross section (CCS) range (~1750−3800 $Å^2$), supporting the conformational diversity across the charge state distribution. These characteristic features are well-known and consistent with intrinsically disordered proteins.[64,65] Most of the α-synuclein glycoforms displayed characteristic ion mobility features, for which the GlcNAc position influences the intramolecular network, leading to conformational changes (Figure 2b). However, while the structural changes in GlcNAcT72 (green), GlcNAcT75 (blue), GlcNAcT81 (purple), and GlcNAcS87 (red) provided signature mobility profiles, only a partial ion mobility separation was obtained at the protein level, as illustrated in Figure 2b. TIMS-MS profiles of α-synuclein and the four glycoforms exhibited large structural heterogeneity and signature patterns across the 8+−15+ charge state distribution

Top-Down ECD MS/MS Analysis of α-Synuclein Glycoforms.

The unmodified α-synuclein sequence and GlcNAc PTM position on each of the α-synuclein glycoforms were confirmed using top-down MS experiments. The ECD MS/MS spectra of the quadrupole isolated $[M + 11H]^{11+}$ (m/z 1314.7) molecular ions of unmodified α-synuclein (magenta) and the GlcNAcT72 (green), GlcNAcT75 (blue), GlcNAcT81 (purple), and GlcNAcS87 (red) glycoforms (m/z 1333.2) are illustrated in Figure S2. Inspection of the ECD MS/MS spectra showed typical $c_i'/z_j^{\bullet}$ product ions with a sequence coverage of ~82%. The ECD fragmentation patterns showed [c_3' to c_{71}'] and [$z_4^{\bullet}$ to $z_{52}^{\bullet}$] product ions without any mass shift, indicating that all serine and threonine residues in these regions are not carrying the GlcNAc PTM. Reporter product ions were obtained for each α-synuclein glycoforms; a characteristic mass shift of 203 Da was obtained between [c_{72}' to c_{139}']/[$z_{72}^{\bullet}$ to $z_{139}^{\bullet}$],[c_{75}' to c_{139}']/[$z_{72}^{\bullet}$ to $z_{139}^{\bullet}$],[c_{82}' to c_{139}']/[$z_{65}^{\bullet}$ to $z_{139}^{\bullet}$], and [c_{87}' to c_{139}']/[$z_{65}^{\bullet}$ to $z_{139}^{\bullet}$] fragment ions, supporting the presence of GlcNAc PTMs at Thr72, Thr75, Thr81, and Ser87 residues, respectively (Figure S2).

Top-Down UVPD MS Analysis of α-Synuclein Glycoforms.

The integration of the UVPD trap prior to the TIMS 2 allowed for additional top-down MS using 213 nm UVPD fragmentation capabilities without mass selection (Figure S1). The UVPD MS spectra of intact α-synuclein GlcNAcT72 (green), GlcNAcT75 (blue), GlcNAcT81 (purple), and GlcNAcS87 (red) glycoforms are illustrated in Figure S3. Typical

$a_i, b_i, c_i / x_j, y_j, z_j$ product ions were observed with a sequence coverage of ~68%. The UVPD and ECD-based top-down MS were found to be consistent in terms of GlcNAc PTM assignments. The low abundance of the reporter UVPD fragment ions did not allow additional tandem ion mobility-selected ECD experiments, as compared to previously studied histone proteoforms (Figure S3).[55]

Middle-Down TIMS-MS Analysis of α-Synuclein Glycoforms.

A middle-down approach was considered using chymotrypsin (Figure 3). Note that chymotrypsin was selected due to the low number of aromatic residues, favoring the generation of middle-down peptide size. The middle-down TIMS-MS analysis resulted in the observation of seven proteolytic peptide fragments: Met5-Tyr39 (35 residues, 3546.9 Da, dark green), Met1-Tyr39 (39 residues, 4039.2 Da, light blue), Val40-Phe94 (55 residues, 5468.9 Da, dark blue), Val95-Tyr125 (31 residues, 3427.6 Da, light purple), Val40-Tyr125 (86 residues, 8878.5 Da, brown), Glu126-Tyr133 (8 residues, 940.4 Da, pink), and Gln134-Ala140 (7 residues, 850.3 Da, light green). Among the seven proteolytic peptide fragments, Val40-Phe94 is of particular importance since it contains all four GlcNAc PTM sites(Figure 3) and comprises the entire NAC region responsible for the protein aggregation. Note that the Met1-Tyr39, Val95-Tyr125, and Glu126-Tyr133 α-synuclein fragments did not show any GlcNAc PTMs at serine and threonine residues, in good agreement with the top-down MS experiments.

The ion mobility and m/z isolation of the peptide molecular ion of interest removed potential isobaric interferences prior to ECD fragmentation. A charge state distribution, ranging from $[M + 4H]^{4+}$ to $[M + 6H]^{6+}$ molecular ion species, was observed for the Val40-Phe94 peptide. TIMS mobility profiles of the Val40-Phe94 proteolytic peptides, carrying the GlcNAc PTM sites, exhibited large conformational heterogeneity across the charge state distribution, for which characteristic ion mobility features (i.e., CCS and number of IMS bands) were observed between the glycoforms (Figure 4). The $[M + 4H]^{4+}$ molecular species of the Val40-Phe94 glycoforms with GlcNAcT72 (green), GlcNAcT75 (blue), GlcNAcT81 (purple), and GlcNAcS87 (red) were separated in the ion mobility domain using a TIMS scan rate of Sr ≤0.14 V/ms (Figure 4). The $[M + 5H]^{5+}$ and $[M + 6H]^{6+}$ molecular species showed a large conformational heterogeneity with higher ion mobility overlap across the positional isomers.

To further evaluate the analytical power of this approach, binary mixtures were considered using GlcNAcT72 (green)/GlcNAcT81 (purple; Figure S4) and GlcNAcT72 (green)/ GlcNAcT75 (blue, Figure 5) glycoforms. A TIMS scan rate of Sr ≤0.14 V/ms was sufficient to baseline separate GlcNAcT72 and GlcNAcT81 (apparent mobility resolving power (R) of ~115, Figure S4a). Moreover, a slower TIMS scan rate of Sr ≤0.07 V/ms was required to separate ion mobility GlcNAcT72 from GlcNAcT75 (apparent mobility R ~180, Figure 5a). The ion mobility and m/z-selected ECD MS/MS spectra of the $[M + 4H]^{4+}$ molecular species (m/z 1368.2) for GlcNAcT72/GlcNAcT75 and GlcNAcT72/ GlcNAcT81 are illustrated in Figure 5b and Figure S4b, respectively. The assigned ECD MS/MS product ions accounted for a sequence coverage of ~83% for all glycoforms. The [c_4' to c_{32}'/c_{36}' to c_{54}']/[$z_6^\bullet$ to$z_{19}^\bullet/z_{37}^\bullet$ to $z_{54}^\bullet$] and [c_4' to c_{32}'/c_{42}' to c_{54}']/[$z_6^\bullet$

to $z_7^{\bullet}/z_{37}^{\bullet}$ to $z_{54}^{\bullet}$] product ions were common between GlcNAcT72/GlcNAcT75 and GlcNAcT72/GlcNAcT81, respectively. Moreover, reporter $c_i'/z_j^{\bullet}$ fragments were observed for the Val40-Phe94 GlcNAc peptide positional isomers, including [c_{33}' to c_{35}']/[$z_{22}^{\bullet}$] for GlcNAcT72/GlcNAcT75 and [c_{33}' to c_{40}']/[$z_{15}^{\bullet}$ to $z_{22}^{\bullet}$] for GlcNAcT72/GlcNAcT81 (Figure 5b). Inspection of the ion mobility and m/z-selected ECD MS/MS spectra of the GlcNAcT72/GlcNAcT75 binary mixtures confirmed the GlcNAc PTM position for IMS bands 1 (GlcNAcT75) and 3 (GlcNAcT75) and for IMS band 2 (GlcNAcT72). Analogously, the ion mobility and m/z-selected ECD MS/MS spectra of the GlcNAcT72/GlcNAcT81 binary mixtures confirmed the GlcNAc PTM position for IMS band 1 (GlcNAcT81) and for IMS band 2 (GlcNAcT72).

The present workflow allowed for clear ion mobility separation and localization of the O-GlcNAc sites for the α-synuclein glycoforms. Although the top-down approach was limited in terms of ion mobility separation between the positional glycoforms, the middle-down strategy using chymotrypsin presented the advantage of digesting α-synuclein into large peptide fragments, and more specifically the digested Val40-Phe94 peptide, which comprises the entire NAC region (highlighted in yellow in Figure 1a) responsible for the protein aggregation. In addition, the middle-down strategy exhibited better sensitivity and ion mobility separation as well as accounted for higher sequence coverage when compared to the top-down approach. However, potential challenges for direct ion mobility-based middle-down ExD analysis are (1) the need for preconcentration due to the lack of chromatography-based techniques combined with relatively low ECD fragmentation efficiency and (2) need for high-resolution ion mobility to separate more complex glycoforms (e.g., containing multiple O-GlcNAc per glycoform).

CONCLUSIONS

The potential of top- and middle-down MS using TIMS in tandem with ECD, UVPD, and ToF MS/MS was demonstrated for the first time for the comprehensive characterization of α-synuclein positional isomers containing single O-GlcNAc modifications (e.g., T72, T75, T81, and S87). The mobility analysis at the protein level provided partial mobility separation of the intact glycoforms, where characteristic/signature IMS bands were observed as a function of the charge state distribution. This is also the first report of top-down ECD and 213 nm UVPD of O-GlcNAc modified proteins; both techniques provided high sequence coverage (over 80%) and unambiguous localization of the O-GlcNAc position.

The online nESI-TIMS-q-ECD-ToF MS/MS analysis of chymotrypsin treated α-synuclein positional isomers, containing a single O-GlcNAc modification, resulted in the unambiguous identification of all four positional isomers. A proteolytic peptide comprising the entire NAC region responsible for the protein aggregation with site modifications (Val40-Phe94) enabled the positional isoform identification in their mixture.

Middle-down ECD provided high sequence coverage and unambiguous localization of the O-GlcNAc modification. The need for high-resolution trapped ion mobility spectrometry was shown for the case of some positional isomers where their separation requires an apparent mobility resolving power higher than ~180).

This first demonstration of top- and/or middle-down technology can be extended to clinical screening for α-synuclein-modified O-GlcNAc to further evaluate the biological activity (e.g., neurotoxicity). The shorter analysis time when compared to chromatography-based workflows makes these approaches more valuable and cost-effective.

Supplementary Material

Refer to Web version on PubMed Central for supplementary material.

ACKNOWLEDGMENTS

The authors acknowledge the financial support from the National Institute of General Medicine grants R01GM134247-01 to F.F.-L. and R01GM114537 to M.R.P.

Data Availability Statement

Top- and Middle-Down raw data of α-synuclein for all five proteoforms are freely accessible at 10.34703/gzx1-9v95/IPFSVI

REFERENCES

(1). Lashuel HA; Overk CR; Oueslati A; Masliah E Nat. Rev. Neurosci 2013, 14 (1), 38–48. [PubMed: 23254192]

(2). Bernal-Conde LD; Ramos-Acevedo R; Reyes-Hernández MA; Balbuena-Olvera AJ; Morales-Moreno ID; Argüero-Sánchez R; Schüle B; Guerra-Crespo M Front. Neurosci 2020, 13, 1399. [PubMed: 32038126]

(3). Stephens AD; Zacharopoulou M; Kaminski Schierle GS Trends Biochem. Sci 2019, 44 (5), 453–466. [PubMed: 30527975]

(4). Liu C; Zhao Y; Xi H; Jiang J; Yu Y; Dong W Front. Cell Neurosci 2021, 15, No. 633727.

(5). Braun AR; Lacy MM; Ducas VC; Rhoades E; Sachs JN J. Membr. Biol 2017, 250 (2), 183–193. [PubMed: 28239748]

(6). Farzadfard A; Pedersen JN; Meisl G; Somavarapu AK; Alam P; Goksoyr L; Nielsen MA; Sander AF; Knowles TPJ; Pedersen JS; Otzen DE Commun. Biol 2022, 5 (1), 123. [PubMed: 35145226]

(7). Emamzadeh FN J. Res. Med. Sci 2016, 21, 29. [PubMed: 27904575]

(8). Giasson BI; Murray IV; Trojanowski JQ; Lee VM J. Biol. Chem 2001, 276 (4), 2380–2386. [PubMed: 11060312]

(9). Cascella R; Perni M; Chen SW; Fusco G; Cecchi C; Vendruscolo M; Chiti F; Dobson CM; De Simone A ACS Chem. Biol 2019, 14 (6), 1352–1362. [PubMed: 31050886]

(10). Stefanis L Cold Spring Harb. Perspect. Med 2012, 2 (2), a009399. [PubMed: 22355802]

(11). Srinivasan E; Chandrasekhar G; Chandrasekar P; Anbarasu K; Vickram AS; Karunakaran R; Rajasekaran R; Srikumar PS Front. Med 2021, 8, No. 736978.

(12). Maries E; Dass B; Collier TJ; Kordower JH; Steece-Collier K Nat. Rev. Neurosci 2003, 4 (9), 727–738. [PubMed: 12951565]

(13). Twohig D; Nielsen HM Mol. Neurodegener 2019, 14 (1), 23. [PubMed: 31186026]

(14). Crews L; Tsigelny I; Hashimoto M; Masliah E Neurotox. Res 2009, 16 (3), 306–317. [PubMed: 19551456]

(15). Kim WS; Kagedal K; Halliday GM Alzheimers Res. Ther 2014, 6 (5), 73. [PubMed: 25580161]

(16). Spillantini MG; Schmidt ML; Lee VM; Trojanowski JQ; Jakes R; Goedert M Nature 1997, 388 (6645), 839–840. [PubMed: 9278044]

(17). Levine PM; Galesic A; Balana AT; Mahul-Mellier AL; Navarro MX; De Leon CA; Lashuel HA; Pratt MR Proc. Natl. Acad. Sci. U.S.A 2019, 116 (5), 1511–1519. [PubMed: 30651314]

(18). Marotta NP; Lin YH; Lewis YE; Ambroso MR; Zaro BW; Roth MT; Arnold DB; Langen R; Pratt MR Nat. Chem 2015, 7 (11), 913–920. [PubMed: 26492012]

(19). Schmid AW; Fauvet B; Moniatte M; Lashuel HA Mol. Cell. Proteomics 2013, 12 (12), 3543–3558. [PubMed: 23966418]

(20). Wang Z; Park K; Comer F; Hsieh-Wilson LC; Saudek CD; Hart GW Diabetes 2009, 58 (2), 309–317. [PubMed: 18984734]

(21). Wang S; Yang F; Petyuk VA; Shukla AK; Monroe ME; Gritsenko MA; Rodland KD; Smith RD; Qian WJ; Gong CX; Liu T J. Pathol 2017, 243 (1), 78–88. [PubMed: 28657654]

(22). Morris M; Knudsen GM; Maeda S; Trinidad JC; Ioanoviciu A; Burlingame AL; Mucke L Nat. Neurosci 2015, 18 (8), 1183–1189. [PubMed: 26192747]

(23). Huynh VN; Wang S; Ouyang X; Wani WY; Johnson MS; Chacko BK; Jegga AG; Qian WJ; Chatham JC; Darley-Usmar VM; Zhang J Front. Aging 2021, 2, No. 757801.

(24). Zhang S; Zhu R; Pan B; Xu H; Olufemi MF; Gathagan RJ; Li Y; Zhang L; Zhang J; Xiang W; Kagan EM; Cao X; Yuan C; Kim SJ; Williams CK; Magaki S; Vinters HV; Lashuel HA; Garcia BA; James Petersson E; Trojanowski JQ; Lee VM; Peng C Nat. Neurosci 2023, 26 (2), 213–225. [PubMed: 36690898]

(25). Permanne B; Sand A; Ousson S; Neny M; Hantson J; Schubert R; Wiessner C; Quattropani A; Beher D ACS Chem. Neurosci 2022, 13 (8), 1296–1314. [PubMed: 35357812]

(26). Pons ML; Loftus N; Vialaret J; Moreau S; Lehmann S; Hirtz C Front. Aging Neurosci 2022, 14, No. 818606.

(27). Avelar AJ; Juliano SA; Garris PA J. Neurochem 2013, 125 (3), 373–385. [PubMed: 23406303]

(28). McFarland MA; Ellis CE; Markey SP; Nussbaum RL Mol. Cell. Proteomics 2008, 7 (11), 2123–2137. [PubMed: 18614564]

(29). Nicholson SJ; Hartson SD; Puterka GJ J. Proteomics 2012, 75 (7), 2252–2268. [PubMed: 22348819]

(30). Phillips AS; Gomes AF; Kalapothakis JM; Gillam JE; Gasparavicius J; Gozzo FC; Kunath T; MacPhee C; Barran PE Analyst 2015, 140 (9), 3070–3081. [PubMed: 25756329]

(31). Seetaloo N; Zacharopoulou M; Stephens AD; Kaminski Schierle GS; Phillips JJ Anal. Chem 2022, 94 (48), 16711–16719. [PubMed: 36413494]

(32). Zhurov KO; Fornelli L; Wodrich MD; Laskay UA; Tsybin YO Chem. Soc. Rev 2013, 42 (12), 5014–5030. [PubMed: 23450212]

(33). Kim MS; Pandey A Proteomics 2012, 12 (4–5), 530–542. [PubMed: 22246976]

(34). Riley NM; Coon JJ Anal. Chem 2018, 90 (1), 40–64. [PubMed: 29172454]

(35). Jeacock K; Chappard A; Gallagher KJ; Mackay CL; Kilgour DPA; Horrocks MH; Kunath T; Clarke DJ J. Am. Soc. Mass Spectrom 2023, 34, 847. [PubMed: 36976861]

(36). Wongkongkathep P; Han JY; Choi TS; Yin S; Kim HI; Loo JA J. Am. Soc. Mass Spectrom 2018, 29 (9), 1870–1880. [PubMed: 29951842]

(37). Wang Z; Udeshi ND; O'Malley M; Shabanowitz J; Hunt DF; Hart GW Mol. Cell. Proteomics 2010, 9 (1), 153–160. [PubMed: 19692427]

(38). Zhao P; Viner R; Teo CF; Boons GJ; Horn D; Wells L J. Proteome Res 2011, 10 (9), 4088–4104. [PubMed: 21740066]

(39). Voinov VG; Deinzer ML; Barofsky DF Rapid Commun. Mass Spectrom 2008, 22 (19), 3087–3088. [PubMed: 18767023]

(40). Voinov VG; Beckman JS; Deinzer ML; Barofsky DF Rapid Commun. Mass Spectrom 2009, 23 (18), 3028–3030. [PubMed: 19685479]

(41). Voinov VG; Deinzer ML; Barofsky DF Anal. Chem 2009, 81 (3), 1238–1243. [PubMed: 19117494]

(42). Voinov VG; Bennett SE; Beckman JS; Barofsky DF J. Am. Soc. Mass Spectrom 2014, 25 (10), 1730–1738. [PubMed: 25037842]

(43). Voinov VG; Bennett SE; Barofsky DF J. Am. Soc. Mass Spectrom 2015, 26 (5), 752–761. [PubMed: 25652934]

(44). Voinov VG; Deinzer ML; Beckman JS; Barofsky DF J. Am. Soc. Mass Spectrom 2011, 22 (4), 607–611. [PubMed: 21472599]

(45). Voinov VG; Hoffman PD; Bennett SE; Beckman JS; Barofsky DF J. Am. Soc. Mass Spectrom 2015, 26 (12), 2096–2104. [PubMed: 26266643]

(46). Fort KL; Cramer CN; Voinov VG; Vasil'ev YV; Lopez NI; Beckman JS; Heck AJR J. Proteome Res 2018, 17 (2), 926–933. [PubMed: 29249155]

(47). Shaw JB; Malhan N; Vasil'ev YV; Lopez NI; Makarov A; Beckman JS; Voinov VG Anal. Chem 2018, 90 (18), 10819–10827. [PubMed: 30118589]

(48). Burnum-Johnson KE; Zheng X; Dodds JN; Ash J; Fourches D; Nicora CD; Wendler JP; Metz TO; Waters KM; Jansson JK; Smith RD; Baker ES Trends Anal. Chem 2019, 116, 292–299.

(49). Zhong Y; Hyung SJ; Ruotolo BT Expert Rev. proteom 2012, 9 (1), 47–58.

(50). Shliaha PV; Gorshkov V; Kovalchuk SI; Schwammle V; Baird MA; Shvartsburg AA; Jensen ON Anal. Chem 2020, 92 (3), 2364–2368. [PubMed: 31935065]

(51). Wei J; Wu J; Tang Y; Ridgeway ME; Park MA; Costello CE; Zaia J; Lin C Anal. Chem 2019, 91 (4), 2994–3001. [PubMed: 30649866]

(52). Gadkari VV; Ramirez CR; Vallejo DD; Kurulugama RT; Fjeldsted JC; Ruotolo BT Anal. Chem 2020, 92 (23), 15489–15496. [PubMed: 33166123]

(53). Williams JP; Morrison LJ; Brown JM; Beckman JS; Voinov VG; Lermyte F Anal. Chem 2020, 92 (5), 3674–3681. [PubMed: 31999103]

(54). Jeanne Dit Fouque K; Kaplan D; Voinov VG; Holck FHV; Jensen ON; Fernandez-Lima F Anal. Chem 2021, 93 (27), 9575–9582. [PubMed: 34170114]

(55). Jeanne Dit Fouque K; Miller SA; Pham K; Bhanu NV; Cintron-Diaz YL; Leyva D; Kaplan D; Voinov VG; Ridgeway ME; Park MA; Garcia BA; Fernandez-Lima F Anal. Chem 2022, 94 (44), 15377–15385. [PubMed: 36282112]

(56). Galesic A; Pratt MR Methods Mol. Biol 2020, 2133, 313–326. [PubMed: 32144674]

(57). Miller SA; Jeanne Dit Fouque K; Ridgeway ME; Park MA; Fernandez-Lima F J. Am. Soc. Mass Spectrom 2022, 33 (7), 1267–1275. [PubMed: 35658468]

(58). Jeanne Dit Fouque K; Wellmann M; Leyva Bombuse D; Santos-Fernandez M; Cintron-Diaz YL; Gomez-Hernandez ME; Kaplan D; Voinov VG; Fernandez-Lima F Anal. Methods 2021, 13 (43), 5216–5223. [PubMed: 34698320]

(59). Marty MT; Baldwin AJ; Marklund EG; Hochberg GK; Benesch JL; Robinson CV Anal. Chem 2015, 87 (8), 4370–4376. [PubMed: 25799115]

(60). Hernandez DR; Debord JD; Ridgeway ME; Kaplan DA; Park MA; Fernandez-Lima F Analyst 2014, 139 (8), 1913–1921. [PubMed: 24571000]

(61). Ridgeway ME; Lubeck M; Jordens J; Mann M; Park MA Int. J. Mass Spectrom 2018, 425, 22–35.

(62). Michelmann K; Silveira JA; Ridgeway ME; Park MA J. Am. Soc. Mass Spectrom 2015, 26 (1), 14–24. [PubMed: 25331153]

(63). Silveira JA; Michelmann K; Ridgeway ME; Park MA J. Am. Soc. Mass Spectrom 2016, 27 (4), 585–595. [PubMed: 26864793]

(64). Beveridge R; Chappuis Q; Macphee C; Barran P Analyst 2013, 138 (1), 32–42. [PubMed: 23108160]

(65). Stuchfield D; Barran P Curr. Opin. Chem. Biol 2018, 42, 177–185. [PubMed: 29428839]

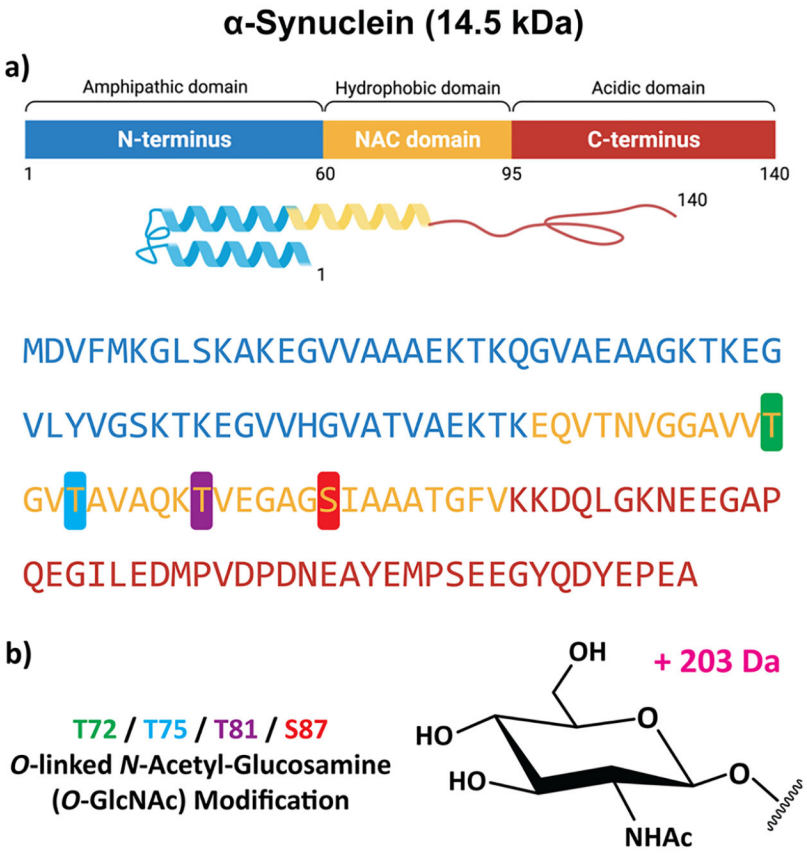

Figure 1.

(a) Schematic, tertiary structure, and sequence of the α-synuclein monomer, showing the N-terminal amphipathic (blue), hydrophobic nonamyloid β-component of plaque (NAC, yellow), and acidic unstructured C-terminal (red) domains. (b) The structure and position of the single O-GlcNAc modification at T72 (green), T75 (blue), T81 (purple), and S87 (red).

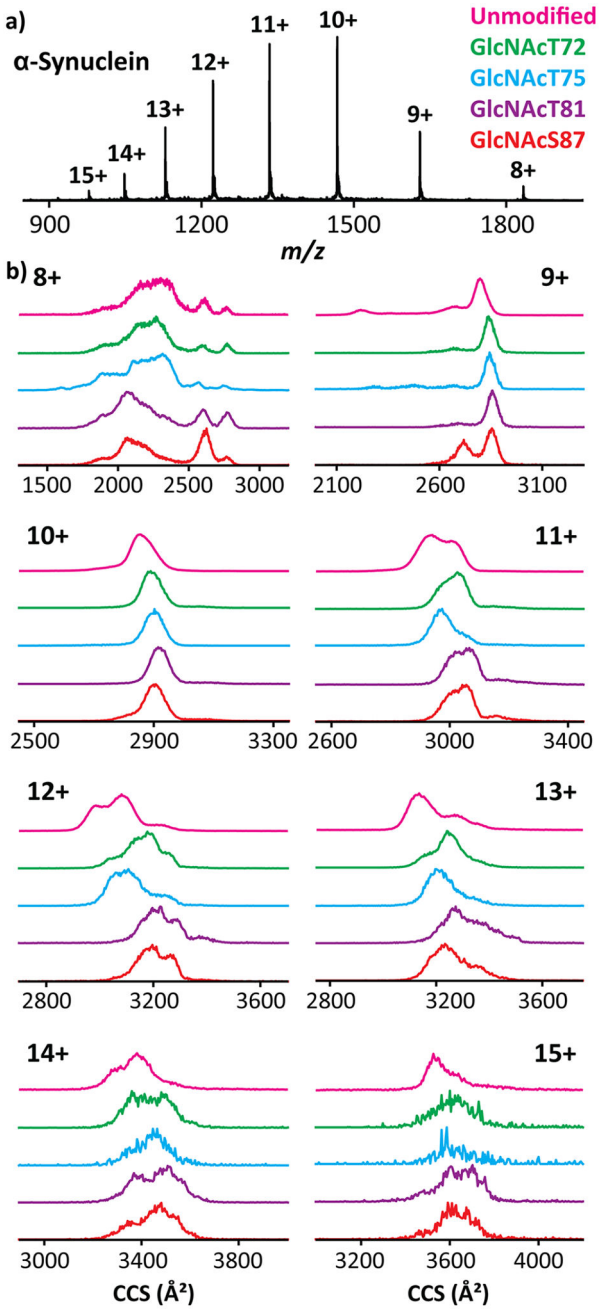

Figure 2.

nESI TIMS-MS analysis showing native (a) MS and (b) TIMS mobility profiles ($^{TIMS}CCS_{N2}$) for α-synuclein unmodified (magenta), GlcNAcT72 (green), GlcNAcT75 (blue), GlcNAcT81 (purple), and GlcNAcS87 (red) glycoforms.

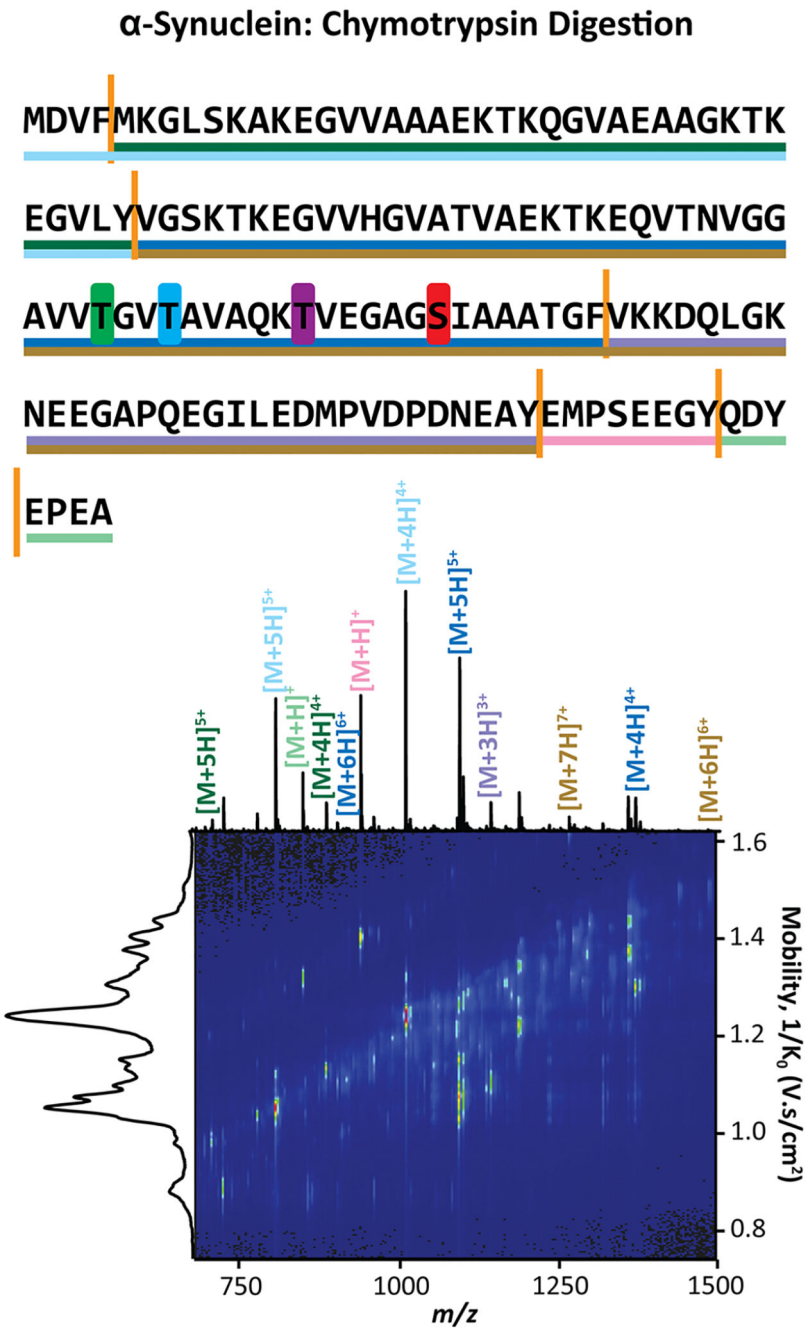

Figure 3.

Middle-down TIMS-MS analysis showing the α-synuclein sequence map as well as the directly infused 2D nESI-TIMS-MS contour map of the peptide fragments obtained using chymotrypsin digestion.

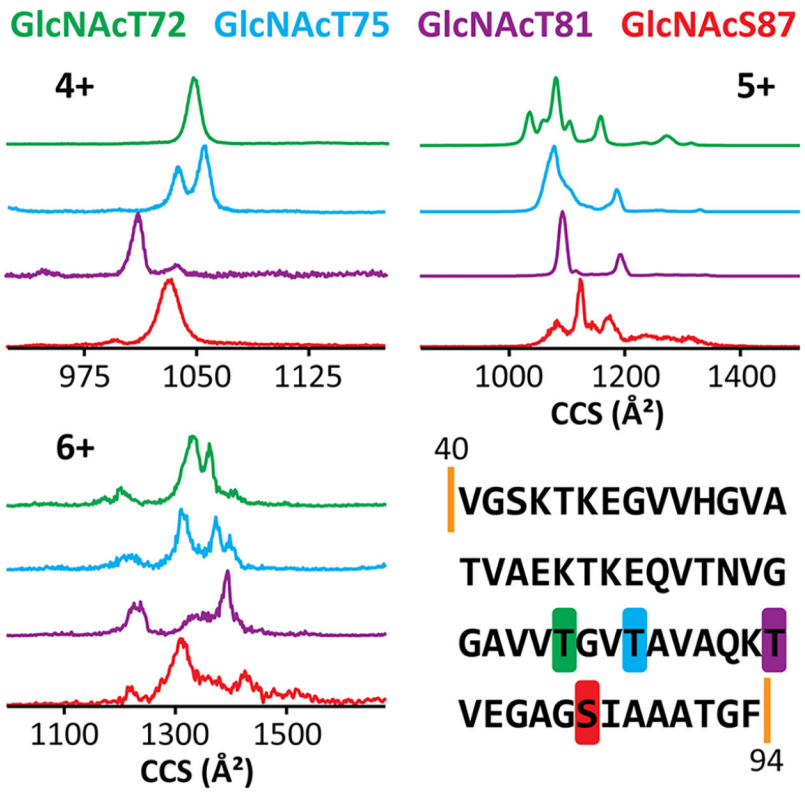

Figure 4.

nESI TIMS-MS analysis showing the TIMS mobility profiles for the α-synuclein proteolytic Val40-Phe94 peptide carrying the GlcNAc PTM sites: GlcNAcT72 (green), GlcNAcT75 (blue), GlcNAcT81 (purple), and GlcNAcS87 (red) glycoforms.

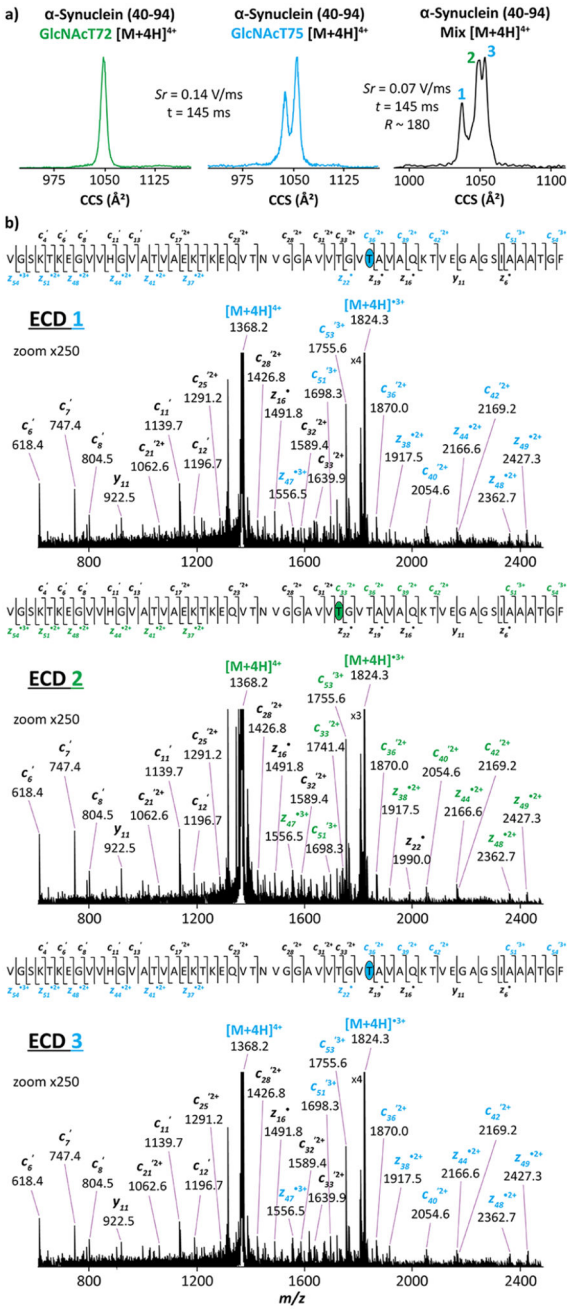

Figure 5.

TIMS-ECD analysis showing the (a) TIMS mobility profiles ($^{TIMS}CCS_{N2}$) of α-synuclein Val40-Phe94 GlcNAcT72 (green) and GlcNAcT75 (blue) with the binary mixture (black) and (b) ion mobility-selected ECD spectra of the selected $[M + 4H]^{4+}$ species of GlcNAcT72 and GlcNAcT75 (m/z 1368.2). The fragments comprising the PTM are highlighted in green and blue for GlcNAcT72 and GlcNAcT75, respectively.